Classification of cardiac cohorts based on morphological and hemodynamic features derived from 4D PC-MRI data

Uli Niemann*§, Atrayee Neog*, Benjamin Behrendt*, Kai Lawonn†, Matthias Gutberlet‡, Myra Spiliopoulou*, Bernhard Preim*, and Monique Meuschke*
* Faculty of Computer Science, Otto von Guericke University Magdeburg, Germany
† Institute of Computer Science, University of Jena, Germany
‡ Heart Centre, University of Leipzig, Germany
§ Corresponding author: uli.niemann@ovgu.de

***Abstract*—An accurate assessment of the cardiovascular system and prediction of cardiovascular diseases (CVDs) are crucial. Cardiac blood flow data provide insights about patient-specific hemodynamics. However, there is a lack of machine learning approaches for a feature-based classification of heart-healthy people and patients with CVDs. In this paper, we investigate the potential of morphological and hemodynamic features extracted from measured blood flow data in the aorta to classify heart-healthy volunteers (HHV) and patients with bicuspid aortic valve (BAV). Furthermore, we determine features that distinguish male vs. female patients and elderly HHV vs. BAV patients. We propose a data analysis pipeline for cardiac status classification, encompassing feature selection, model training, and hyperparameter tuning. Our results suggest substantial differences in flow features of the aorta between HHV and BAV patients. The excellent performance of the classifiers separating between elderly HHV and BAV patients indicates that aging is not associated with pathological morphology and hemodynamics. Our models represent a first step towards automated diagnosis of CVS using interpretable machine learning models.**

***Index Terms*—cardiovascular disease, bicuspid aortic valve, machine learning, feature selection**

I. Introduction

Worldwide, most people die of cardiovascular diseases (CVDs) [1]. Therefore, an accurate assessment of the cardiovascular system and prediction of CVDs are crucial. There appear to be relationships between hemodynamics and cardiac pathologies [2], [3] for which patient-specific flow information is required. Time-dependent flow data in a 3D volume can be acquired non-invasively using four-dimensional phase-contrast magnetic resonance imaging (4D PC-MRI) [4]. The flow information can be evaluated in any vessel section. Thus, 4D PC-MRI has great potential to improve the diagnosis, follow-up, and treatment decisions of CVDs.

There are visual exploration techniques for single 4D PC-MRI data sets [5], [6] involving different time-dependent flow features. However, developing guidelines on interpreting 4D PC-MRI data requires the analysis of cohorts instead of single data sets. Therefore, we study how reliable we can predict disease status with supervised classification models learned on morphological and hemodynamic features extracted from 4D PC-MRI data of heart-healthy volunteers (HHV) and patients with bicuspid aortic valve (BAV). To support physicians in diagnosing and assessing the severity of BAV defects and understanding better the variety of physiological hemodynamic and morphological features, we defined the following research questions. RQ 1: Do heart-healthy volunteers and BAV patients differ regarding the extracted features [7]? RQ 2: Are there predictive features that can separate between elderly heart-healthy volunteers and BAV patients? This question is motivated by the challenge in clinical practice to distinguish between a non-pathological decline in cardiac function with increasing age [8] (*healthy aging*) and the onset of early stages of BAV, solely based on flow velocity. RQ 3: Do female and male heart-healthy volunteers differ w.r.t. morphological and hemodynamic attributes? Since women generally have a smaller heart, a smaller blood volume, and a faster heartbeat than men [9], the identification of further differences related to aortic blood flow might suggest the necessity to stratify diagnostic procedures or treatment pathways by gender. We train separate models for the healthy subgroups and BAV patients based on the combination of several feature selection methods and learning algorithms. Model training is combined with a feature selection step to identify correlations between the multitude of flow features and reduce them to a meaningful subset. Finally, we study and compare the informativeness of each parameter towards the outcomes.

II. Related Work

There is extensive research on machine learning (ML) in cardiology, for example, to support computer-aided diagnosis and prediction of heart diseases [10]. Dinh et al. [11] created a classification model ensemble from different base classifiers in cardiovascular disease diagnosis. They found patient features such as age, blood pressure, body weight, and chest pain to be most predictive. Similarly, Miao et al. [12] trained an ensemble classifier for coronary heart disease diagnosis using data gathered from four different medical institutions. Wojnarski et al. [13] identified three distinct phenotypes of BAV patients based on vascular morphology via data clustering. While

To appear in: Proceedings of the IEEE 35th International Symposium on Computer Based Medical Systems (CBMS)

acknowledging the high potential of ML, Russak et al. [14] observed that case studies of successful integration of these technologies into clinical practice are still sparse. They further suggested guidelines to increase acceptance and ultimately to enable clinical adoption of ML techniques in cardiology, including a project development driven by unsolved clinical questions rather than by the available data only, incorporating experts from multiple disciplines, using complete patient data gathered in a standardized format, improving the interpretability of complex ML models, and training clinicians on ML fundamentals to increase familiarity with these concepts.

Deep learning has become increasingly popular for cardiovascular applications [15]–[17]. In comparison to classic ML algorithms, deep neural networks often exhibit superior accuracy and work on raw image data, thus reducing the necessity to carefully extract features using domain knowledge, which is often too time-consuming or expensive. However, the "black-box" nature of deep neural networks is rather unsuited for inference, which is crucial, especially in medical applications. Thus, some studies create more parsimonious models using interpretable features to understand better characteristics of anatomical structures predictive for the outcome. Niemann et al. [18] studied the potential of 22 morphological features extracted from angiographic images for a data-driven rupture risk classification in intracranial aneurysms. Post-hoc interpretation steps revealed the most predictive features, including a dome point angle, ellipticity index, and aneurysm volume. In addition to morphology, Detmer et al. [19] investigated hemodynamic features and patient features for rupture risk assessment and found that ruptured aneurysms exhibit larger and more complex flow features.

Often, the number of extracted features is large, which often leads to unnecessarily complex models. Selecting a subset of features can help to reduce computational complexity, increase model performance, and enhance model interpretability [20], [21]. For example, Latha et al. [20] combined ensemble classifiers with a preceding feature selection step to improve heart disease prediction accuracy.

III. Medical Background

The aorta is the largest artery in the human vascular system, which allows to measure a meaningful signal for blood flow analysis. During systole, oxygenated blood passes from the left ventricle (LV) via the aortic valve (AV) into the ascending aorta, see Figure 1. From the right ventricle, deoxygenated blood is pumped through the pulmonary valve into the pulmonary artery. During diastole, the AV is closed to prevent blood from flowing back into the LV.

A. BAV and Related Flow Behavior

Hemodynamic parameters are an indicator for the emergence and progression of CVDs. CVDs change the vessel morphology, which promotes flow abnormalities [22]. The bicuspid aortic valve, describing a fusion of two leaflets, is the most common congenital heart defect [23].

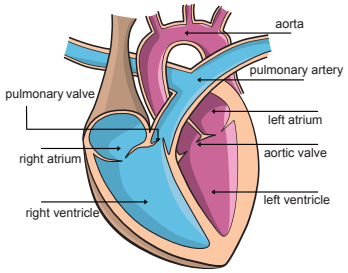

Fig. 1: Anatomy of the human heart.

Several studies investigated the influence of a BAV on flow patterns in the ascending aorta [3], [7], [24]. Compared with healthy volunteers, patients more often had a helical blood flow, often accompanied by an eccentric main blood flow and increased wall shear stress as well as flow velocities and vortex volumes. However, there was no computer support for parameter selection, which made the analysis process time-consuming and error-prone. Thus, a detailed analysis of the flow parameters regarding several cohorts remains a challenge.

B. Data Acquisition and Parameter Extraction

A 3 T MR scanner was used to acquire the 4D PC-MRI data with a maximum expected velocity of 1.5 m/s per dimension. The spatio-temporal resolution is $1.77 \times 1.77 \times 3.5$ mm^3 \ 50 ms resulting in 19 to 35 slices and 18 to 33 time steps.

To analyze a 4D PC-MRI data set, the software *Bloodline* [5] is used. During pre-processing, image artifacts are corrected, and the thoracic aorta is segmented. Then, the aortic flow is automatically calculated based on the MRI data. To evaluate the heart function 197 hemodynamic parameters are computed [5]. A distinction is made between parameters that describe the vortical flow and those representing the laminar flow. In addition, planes were placed along the aorta. For each plane, different properties of the vortical flow are measured, called "in-plane" parameters. The maximum, minimum, median, and mean value per parameter is determined over all planes and time steps. Furthermore, so-called "through-plane" parameters, which characterize the laminar flow, are determined at each plane over time, and the maximum, minimum, median, and mean value per parameter is calculated.

So far, 90 data sets of heart-healthy volunteers and 22 BAV patients have been evaluated with Bloodline. These 112 data sets serve as input for our classification pipeline.

IV. Methods

Our data analysis pipeline is depicted in Figure 2. After extracting the morphological and hemodynamic parameters from raw 4D PC-MRI images, we build separate models for each of three *classification tasks* (CT), i.e., models that distinguish (CT 1) HHV vs. BAV patients, (CT 2) elderly HHV vs. BAV patients and (CT 3) female HHV vs. male HHV. For this purpose, we make use of a wide range of feature selection methods and classification algorithms. This section describes the pipeline's main steps, including data preprocessing, feature selection, classification, and evaluation.

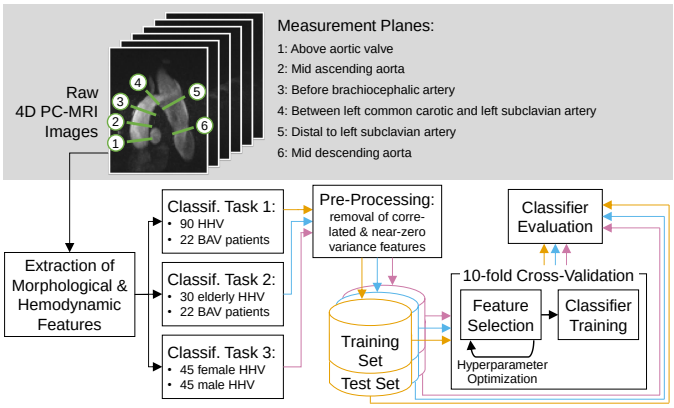

Fig. 2: **Schematic overview of our data analysis pipeline.**

A. Data Pre-Processing

We remove 103 highly correlated features using the algorithm of Kuhn and Johnson [25] with a threshold of 0.9. Secondly, we eliminate near-constant features, where the most frequent value occurs ≥ 20 times as often as the second most frequent value and where the number of unique values is smaller than 10. We remove 3 such features, resulting in a total of 94 features for classification.

For the CT 2, we divide the feature "age" into two intervals, which we refer to as "younger" and "elderly", respectively. We determine the cutoff value as age with maximum information gain [26] towards cardiac status. Discretization leads to a subgroup of 78 younger subjects up to 47 years (60 HHV, 18 BAV patients) and a subgroup of 34 elderly subjects (30 HHV, 4 BAV patients). The data is then split randomly into a training set (70%) and a test (30%) set.

B. Classification Algorithms and Feature Selection

We use the following five classification algorithms: CART decision tree (DT) [27], random forest (RF) [28], gradient boosted trees (GBT) [29], support vector machine (SVM) [30], and least absolute shrinkage and selection operator (LASSO) [31]. We bundle classifier training with a preceding feature selection step to reduce computational complexity, increase model performance, and enhance model interpretability. We use three filter and four wrapper methods: correlation-based feature selection (CFS) filter, χ^2-test filter, information gain filter (IG), sequential forward search (SFS) wrapper, sequential backward search (SBS) wrapper, genetic search (GS) wrapper, and random search (RS) wrapper.

C. Evaluation

We train separate models for each combination of feature selection method (7) and classification algorithm (5), yielding a total of 35 models. Hyperparameter selection for the feature selection methods was performed using 10-fold stratified cross-validation. We use accuracy as the primary evaluation measure for CT 3, which exhibits a balanced class distribution (45 female HHV vs. 45 male HHV). Accuracy (ACC) quantifies the ratio of correctly labeled observations. Due to the class imbalance for the first two CTs (90 HHV vs. 22 BAV patients; 30 elderly HHV vs. 22 BAV patients), we opt for Cohen's kappa, defined as $\kappa = \frac{p_o - p_e}{1 - p_e}$, where p_o represents ACC and p_e is the probability for agreement among the vector of true class labels and the class labels assigned by random prediction. We also report the area under the receiver operating characteristic curve (AUC). A receiver operating characteristic curve illustrates the true positive rate (TPR) and false positive rate (FPR) for different prediction thresholds of a binary classifier. The AUC ranges from 0 (0% TPR, 100% FPR) to 1 (100% TPR, 0% FPR), where a classifier making random predictions achieves an AUC of 0.5.

V. Results

We summarize our classification results in Table I and show the hyperparameter tuning results for feature selection in Table II.

A. CT 1: heart-healthy volunteers (HHV) vs. BAV patients

The best model (SFS + RF) achieves $\kappa = 0.969$ (ACC = 93.9%, AUC = 0.796). Three features were selected:

- *Time-to-Peak-Vorticity*: the time point during the heart cycle where the overall volume of blood swirling within a vortex in the aorta reaches its peak. (in ms; 0 ms = begin of heart cycle).
- *Time-to-Peak-In-Plane-Velocity*: the time point during the heart cycle when the max. velocity of in-plane blood flow occurs in the aorta (ms).
- *Peak-Systolic-In-Plane-Mean-Velocity*: the max. mean in-plane blood flow velocity over all planes and systolic time points (m/s).

Figure 3 highlights considerable differences between HHV and BAV patients for these three features. In particular, BAV patients exhibit a much smaller range in *Time-to-Peak-Vorticity* (min: 130 ms, max: 312 ms) than HHV (min: 0 ms, max: 1573 ms). Similarly, whereas all HHV show a *Peak-Systolic-In-plane-Mean-Velocity* of 0.32 m/s or lower, variability within the BAV subgroup is much larger (min: 0.12 m/s, max: 0.60 m/s).

B. CT 2: elderly HHV vs. BAV patients

The best model (SFS + SVM) correctly classifies all 15 test instances (κ = 1, ACC = 100%, AUC = 1). Five features were selected:

- *Peak-Systolic-Mean-Velocity*: the highest of the mean through-plane blood flow velocities over all planes and systolic time steps during an aortic cardiac cycle (m/s).
- *Time-to-Peak-Systolic-Through-Plane-Mean-Velocity*: the time point during the systole where the mean through-plane velocity over all planes peaks (ms).
- *Time-to-Peak-Diastolic-In-Plane-Mean-Velocity*: the time point during the diastole where the mean in-plane velocity over all planes peaks (ms).
- *Diastolic-Median-Right-Rotation-Volume-Rel*: the median of the volume within the vessel containing right-handed rotational flow over all diastolic time steps relative to the total vessel volume (%).

TABLE I: **Classification results.** For each classification task (CT), the number of features d and test performance of the five best combinations of feature selection method (FS) and classification algorithm (CA) are depicted.

CT	#	FS + CA	d	κ	ACC	AUC
CT 1 HHV vs. BAV patients	1	SFS + RF	3	**0.969**	0.939	0.796
	2	SFS + GBM	3	0.962	0.939	0.819
	3	SFS + SVM	3	0.901	0.969	0.891
	4	SFS + DT	2	0.639	0.878	0.935
	5	CFS + GBM	19	0.796	0.939	0.898
CT 2 elderly HHV vs. BAV patients	1	SFS + SVM	5	**1.000**	1.000	1.000
	2	SFS + RF	3	0.925	0.866	0.722
	3	SFS + DT	1	0.777	0.800	0.571
	4	SFS + GBM	1	0.777	0.800	0.571
	5	CFS + DT	6	0.705	0.866	0.833
CT 3 female HHV vs. male HHV	1	SFS + SVM	3	0.384	**0.692**	0.562
	1	SFS + GBM	3	0.384	**0.692**	0.562
	3	SFS + RF	2	-0.076	**0.692**	0.384
	4	CFS + GBM	3	0.153	0.576	0.577
	5	SFS + DT	2	0.076	0.538	0.553

TABLE II: **Tuning grid of feature selection (FS) hyperparameters.** Optimal values in boldface.

FS	Hyperparameter	Candidate values
χ^2	Relative number of selected features	$\{0, \frac{1}{9}, \frac{2}{9}, \frac{\mathbf{3}}{\mathbf{9}}, \ldots, 1\}$
IG	Relative number of selected features	$\{0, \frac{1}{9}, \frac{2}{9}, \frac{\mathbf{3}}{\mathbf{9}}, \ldots, 1\}$
SFS	Minimum improvement in performance when adding a feature α	$\{0.005, 0.01, \mathbf{0.02}, 0.1\}$
SBS	Maximum decrease in performance when removing a feature β	$\{\mathbf{10^{-3}}, 10^{-2}, 10^{-1}\}$
GS	Number of iterations	$\{\mathbf{10}, 20, 30\}$
GS	Initial number of feature subsets	$\{\mathbf{10}, 15, 20\}$
RS	Number of iterations	$\{10, 50, 100, \mathbf{200}\}$

- *Peak-Mean-Vorticity-Pressure*: the highest mean pressure within vortex regions over all time steps (mmHg).

Figure 4 shows differences in the distribution of *diastolic-Median-Right-Rotation-Volume-Rel* between elderly HHV (mean 0.51 $\pm$ std. dev. 0.01) and BAV patients (0.61 $\pm$ 0.09).

C. CT 3: female vs. male HHV

The combination of SFS and RF achieves best generalization performance (ACC = 69.2%, κ = 0.384, AUC = 0.562), cf. Table I. Just as with the first CT, three features were selected:

- *Peak-Velocity*: the max. velocity of blood flow in the aorta over a cardiac cycle (m/s).
- *Peak-Systolic-VelocityQ99*: the max. velocity of blood flow (taken from the 99.5% quantile range to discard outliers due to noise) that occurs in the aorta during the systolic phase of the cardiac cycle (m/s).
- *Time-to-Peak-Diastolic-Through-Plane-Velocity* the time point during the diastole when the velocity of the through-plane blood flow peaks in any of the planes in the aorta (ms; 0 ms = begin of heart cycle).

Although these three features yield the best model, the plot matrix in Figure 5 shows that female and male HHV have quite similar value distributions.

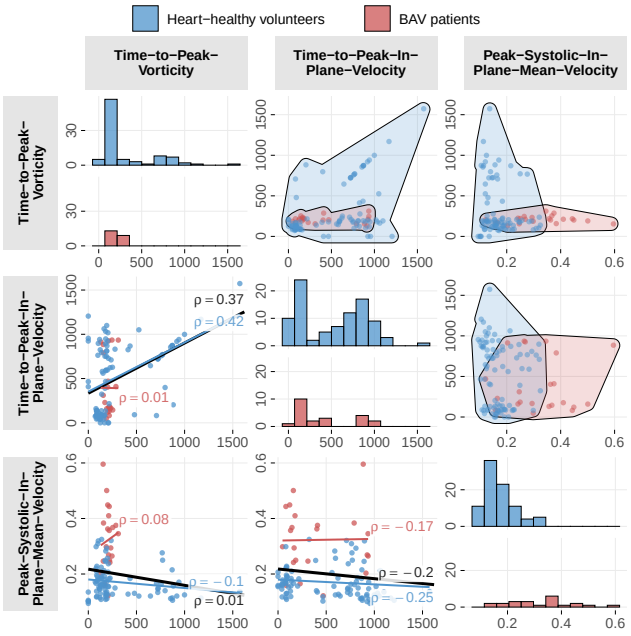

Fig. 3: **Plot matrix for features of the best model for CT 1 (SFS+RF).** Pairwise relationships of the features selected for the best combination of feature selection and classification algorithm are shown for CT 1. Scatterplots illustrate the relationship between the feature labeled at the top of the column (x-axis) and the feature labeled at the left of the row (y-axis). Colored lines illustrate the strength of the linear relationship, and labels display the Spearman correlation coefficient (ρ). Convex hulls illustrate the overlap between the two subgroups in the depicted 2D feature space. Histograms on the main diagonal show the distribution of a feature for each class label.

VI. Discussion

Our classification results suggest substantial differences in aortic flow characteristics between HHV and bicuspid aortic valve (BAV) patients. For several features, BAV patients show higher variation and larger value ranges. To verify the validity of our models, we discussed the results with a radiologist (coauthor) who specializes in cardiac imaging and has 23 years of professional experience. He also provided the data sets.

The possible aortic valve stenosis due to the altered valve morphology in BAV patients means that the heart must exert more force to open the valve and pump the blood further due to this resistance. As a result, flow velocity increases significantly compared to healthy individuals, especially during systole. The substantial increase in flow velocity favors the formation of vortical blood flow within the aorta. Consequently, the forward movement of the flow along the centerline decreases, and there is more flow that rotates within a plane, which is also reflected in the results for CT 1.

The feature *Peak-Systolic-In-Plane-Mean-Velocity* represents the velocity of flow in a plane. In HHV, it is less than 30 cm/min, and the average flow velocity is 1.5 m/sec. Accordingly, the flow velocity in a plane in BAV patients is

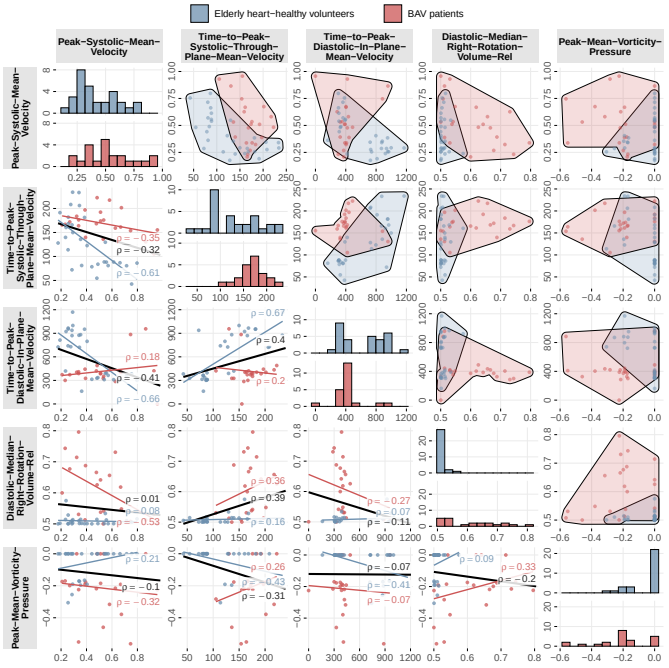

Fig. 4: **Plot matrix of the best model's features for CT 2 (SFS+SVM).** See Figure 3 for a description.

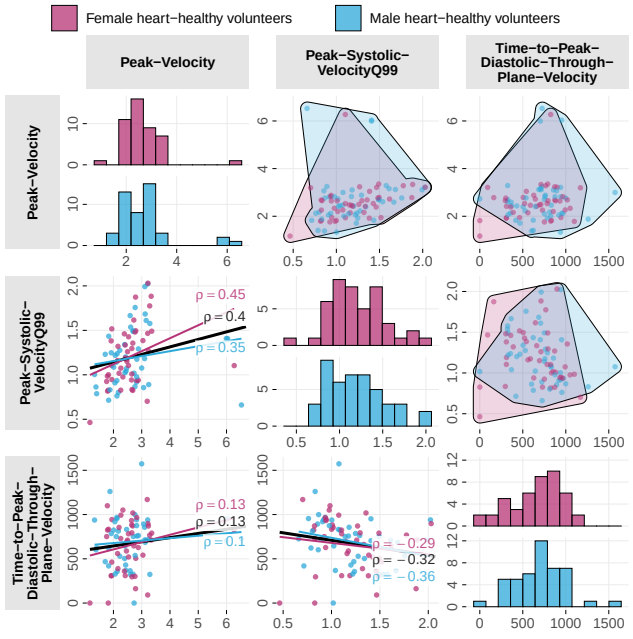

Fig. 5: **Plot matrix for features of the best model for CT 3 (SFS+SVM).** See Figure 3 for a description.

at least one third of the average flow velocity, which is a very high value. These circumstances explain the good separation of HHV and BAV patients based on *Peak-Systolic-In-Plane-Mean-Velocity*. The second feature *Time-to-Peak-In-Plane-Velocity* measures the time of maximum flow velocity in one plane. The radiologist assumes that this is the corresponding time for the *Peak-Systolic-In-Plane-Mean-Velocity*. Due to the high flow velocity in BAV patients, vortical flow occurs earlier during the cardiac cycle. Therefore, the *Time-to-Peak-In-Plane-Velocity* occurs earlier than in healthy volunteers. Nevertheless, the radiologist was pleasantly surprised to find that only a small number of features provided good class separation. He emphasized that determining the corresponding threshold values is of paramount importance to support the diagnosis of CVDs.

Concerning RQ 2, we could not confirm that elderly HHV have similar flow characteristics to BAV patients in the current data set. However, *Diastolic-Median-Right-Rotation-Volume-Rel* seems to provide a good separation of the two groups. In HHV, slight vortical flow occurs only during systole, whereas hardly any vortical flow occurs during diastole because the aortic valve is fully closed, which is also the case in older participants. BAV patients, on the other hand, show increasing vortical flow, even during diastole, which is why a differentiation of both groups was possible here. Since the best models perform excellently with only three to five features, we conclude that our approach to extract interpretable features is useful for diagnosing BAV patients.

Regarding RQ 3, we conclude that although there are minor differences between female and male HHV, morphological and hemodynamic features alone are not sufficient to distinguish the sexes with high accuracy, which was also in accordance with the expectations of our radiologist. Although men have, on average, a larger cardiac and blood volume than women, this does not substantially affect the derived morphological and hemodynamic characteristics. Nevertheless, such detailed analysis of HHV is essential to derive normal values and thus reliably detect abnormal values.

Although we consider our results promising, there are some limitations. First, our data set could be subject to a selection bias. The HHV group includes only volunteers between 18 and 65 years old. Even older subjects were excluded because they already had an enlargement of the aortic diameter that, although not yet requiring treatment, deviated from a physiological morphology. Accordingly, our calculated age cutoff of 47 years for classification of elderly HHV and BAV patients was relatively low, which may explain the good separability. In addition, BAV patients were not differentiated according to pronounced sequelae, aortic valve stenosis, and aortic valve insufficiency. This could also influence the results. We used Information Gain to determine the cutoff value of 47 years and divide the subjects into two age-based subsets. Alternatively, we could have tested multiple thresholds to choose the cutoff value which yields the best classification performance. However, a study of patients with coronary artery disease [32] also showed that patients aged ca. 50 years and older had similar ventricular diastolic filling to the control group, whereas there were greater differences between groups in younger subjects. In addition, our holdout evaluation estimates may be influenced by the relatively small test set, especially for CT 2 where the test set contains only 15 observations. In the future, we would like to expand our data analysis pipeline with a nested-cross validation scheme

that involves tuning of feature selection hyperparameters and calculation of generalization performance simultaneously, thus reducing the variability of the performance estimates.

VII. Conclusion and Future Work

We presented a data analysis pipeline for classification of BAV versus HHV patients. Therefore, we extracted a large number of morphological and hemodynamic parameters from 4D PC-MRI data sets. We integrated various feature selection methods with classifier training to reduce the number of features, aiming to build accurate yet parsimonious classification models. Our results showed differences between BAV patients and HHV with respect to hemodynamics, such as the higher blood flow velocity in BAV patients.

Furthermore, we applied our pipeline to two other classification tasks. First, we investigated whether there are morphological and hemodynamic differences between elderly HHV and BAV patients. We were able to confirm this based on the classifiers' high performance, although our results must be validated on another independent data set. Second, we trained a model that distinguishes between female and male HHV based on the extracted parameters. We did not identify features capable of predicting gender accurately.

In the future, we plan to expand our pipeline to other pathologies, such as diseases of other cardiac vessels, such as tetralogy of Fallot, which primarily involves changes in the pulmonary artery. This may contribute to improving the diagnostic workflow. Furthermore, we want to expand our data collection to include more elderly HHV ($\geq$ 60 years old) to check whether healthy aging people show similar characteristics to BAV patients. Moreover, we plan to evaluate the treatment success, e.g., after an aortic valve replacement, to examine whether the flow normalizes after surgery, by applying our models to new, treated cases. This would provide insights into whether the flow returns to normal after the insertion of an artificial heart valve.

References

[1] S. Mendis, P. Puska, B. Norrving *et al.*, *Global atlas on cardiovascular disease prevention and control*. Geneva: WHO, 2011.

[2] R. Lorenz, J. Bock, (...), and M. Markl, "4D flow magnetic resonance imaging in bicuspid aortic valve disease demonstrates altered distribution of aortic blood flow helicity," *Magn Reson Med*, vol. 71, no. 4, pp. 1542–53, 2014.

[3] A. McNally, A. Madan, and P. Sucosky, "Morphotype-dependent flow characteristics in bicuspid aortic valve ascending aortas: A benchtop particle image velocimetry study," *Front Physiol*, vol. 8, p. 44, 2017.

[4] M. Markl, A. Frydrychowicz, (...), and O. Wieben, "4D flow MRI," *J Magn Reson Imaging*, vol. 36, no. 5, pp. 1015–36, 2012.

[5] B. Köhler, M. Grothoff, M. Gutberlet, and B. Preim, "Bloodline: A system for the guided analysis of cardiac 4D PC-MRI data," *Computers & Graphics*, vol. 82, pp. 32–43, 2019.

[6] E. M. Semaan, M. Carr, (...), and B. Spottiswoode, "Evaluation of an optimized post-processing tool for 4D flow MRI data analysis in healthy volunteers and patients with aortic stenosis, aortic insufficiency, and aortic aneurysm," in *Proc. of ISMRM*, 2014, p. 3948.

[7] S. Ebel, J. Dufke, (...), and M. Gutberlet, "Automated Quantitative Extraction and Analysis of 4D flow Patterns in the Ascending Aorta: An intraindividual comparison at 1.5 T and 3 T," *Scientific Reports*, vol. 10, no. 1, pp. 1–13, 2020.

[8] B. Lernfeit, J. Wikstrand, A. Svanborg, and S. Landahl, "Aging and left ventricular function in elderly healthy people," *American Journal of Cardiology*, vol. 68, no. 5, pp. 547–9, 1991.

[9] M. J. Legato and J. K. Legha, "Gender and the heart: sex-specific differences in normal myocardial anatomy and physiology and in the experiences of some diseases of the cardiovascular system," in *Principles of Gender-Specific Medicine*. Elsevier Inc., 2004, pp. 185–92.

[10] S. J. Al'Aref, K. Anchouche, (...), and J. K. Min, "Clinical applications of machine learning in cardiovascular disease and its relevance to cardiac imaging," *Eur Heart J*, vol. 40, no. 24, pp. 1975–86, 2019.

[11] A. Dinh, S. Miertschin, A. Young, and S. D. Mohanty, "A data-driven approach to predicting diabetes and cardiovascular disease with machine learning," *BMC Med Inform Decis Mak*, vol. 19, no. 1, p. 211, 2019.

[12] K. H. Miao, J. H. Miao, and G. J. Miao, "Diagnosing coronary heart disease using ensemble machine learning," *Int J Adv Comput Sci Appl*, vol. 7, no. 10, pp. 30–9, 2016.

[13] C. M. Wojnarski, E. E. Roselli, (...), and B. W. Lytle, "Machine-learning phenotypic classification of bicuspid aortopathy," *J. Thorac. Cardiovasc. Surg.*, vol. 155, no. 2, pp. 461–9, 2018.

[14] A. J. Russak, F. Chaudhry, (...), and B. S. Glicksberg, "Machine Learning in Cardiology—Ensuring Clinical Impact Lives Up to the Hype," *J Cardiovasc Pharm T*, 2020.

[15] Z. Arabasadi, R. Alizadehsani, (...), and A. A. Yarifard, "Computer aided decision making for heart disease detection using hybrid neural network-genetic algorithm," *Comput Methods Programs Biomed*, vol. 141, pp. 19–26, 2017.

[16] J. K. Kim and S. Kang, "Neural network-based coronary heart disease risk prediction using feature correlation analysis," *J Healthc Eng*, 2017.

[17] C. Martin-Isla, V. M. Campello, (...), and K. Lekadir, "Image-Based Cardiac Diagnosis With Machine Learning: A Review," *Frontiers in Cardiovascular Medicine*, vol. 7, pp. 1–19, 2020.

[18] U. Niemann, P. Berg, (...), and S. Saalfeld, "Rupture Status Classification of Intracranial Aneurysms Using Morphological Parameters," in *Computer-Based Medical Systems (CBMS)*, 2018, pp. 48–53.

[19] F. J. Detmer, B. J. Chung, (...), and J. R. Cebral, "Associations of hemodynamics, morphology, and patient characteristics with aneurysm rupture stratified by aneurysm location," *Neuroradiol*, vol. 61, no. 3, pp. 275–84, 2019.

[20] C. B. C. Latha and S. C. Jeeva, "Improving the accuracy of prediction of heart disease risk based on ensemble classification techniques," *Inform Med Unlocked*, vol. 16, p. 100203, 2019.

[21] Q.-u.-a. Mastoi, T. Y. Wah, R. Gopal Raj, and U. Iqbal, "Automated Diagnosis of Coronary Artery Disease: A Review and Workflow," *Cardiol Res Pract*, 2018.

[22] P. Kilner, G. Yang, (...), and D. B. Longmore, "Helical and Retrograde Secondary Flow Patterns in the Aortic Arch Studied by Three Directional Magnetic Resonance Velocity Mapping," *Circ*, vol. 88, pp. 2235–47, 1993.

[23] C. Ward, "Clinical significance of the bicuspid aortic valve," *Heart*, vol. 83, no. 1, pp. 81–5, 2000.

[24] C. Meierhofer, E. P. Schneider, (...), and S. Fratz, "Wall shear stress and flow patterns in the ascending aorta in patients with bicuspid aortic valves differ significantly from tricuspid aortic valves: a prospective study," *Eur Heart J Cardiovasc Imaging*, vol. 14, no. 8, pp. 797–804, 2013.

[25] M. Kuhn and K. Johnson, *Applied predictive modeling*. Springer, 2013, vol. 26.

[26] J. R. Quinlan, "Induction of decision trees," *Mach Learn*, vol. 1, no. 1, pp. 81–106, 1986.

[27] L. Breiman, J. Friedman, R. Olshen, and C. Stone, *Classification and Regression Trees*. Wadsworth and Brooks, 1984.

[28] L. Breiman, "Random forests," *Machine learning*, vol. 45, no. 1, pp. 5–32, 2001.

[29] J. H. Friedman, "Greedy function approximation: a gradient boosting machine," *Ann Stat*, pp. 1189–232, 2001.

[30] B. E. Boser, I. M. Guyon, and V. N. Vapnik, "A training algorithm for optimal margin classifiers," in *Proc. of Workshop on Computational Learning Theory*, 1992, pp. 144–52.

[31] J. Friedman, T. Hastie, and R. Tibshirani, "Regularization paths for generalized linear models via coordinate descent," *J Stat Softw*, vol. 33, no. 1, pp. 1–22, 2010.

[32] H. Kuecherer and K. Ruffmann, "Effect of aging on doppler echocardiography filling parameters in normal subjects and in patients with coronary artery disease," *Clin. Cardiol.*, vol. 11, no. 5, pp. 303–6, 1988.